Cell Reports, Volume *42*

Supplemental information

Targeting MCL-1 triggers DNA damage and an anti-proliferative response independent from apoptosis induction

Utsarga Adhikary, Joao A. Paulo, Marina Godes, Shrabasti Roychoudhury, Michelle S. Prew, Yael Ben-Nun, Ellen W. Yu, Amit Budhraja, Joseph T. Opferman, Dipanjan Chowdhury, Steven P. Gygi, and Loren D. Walensky

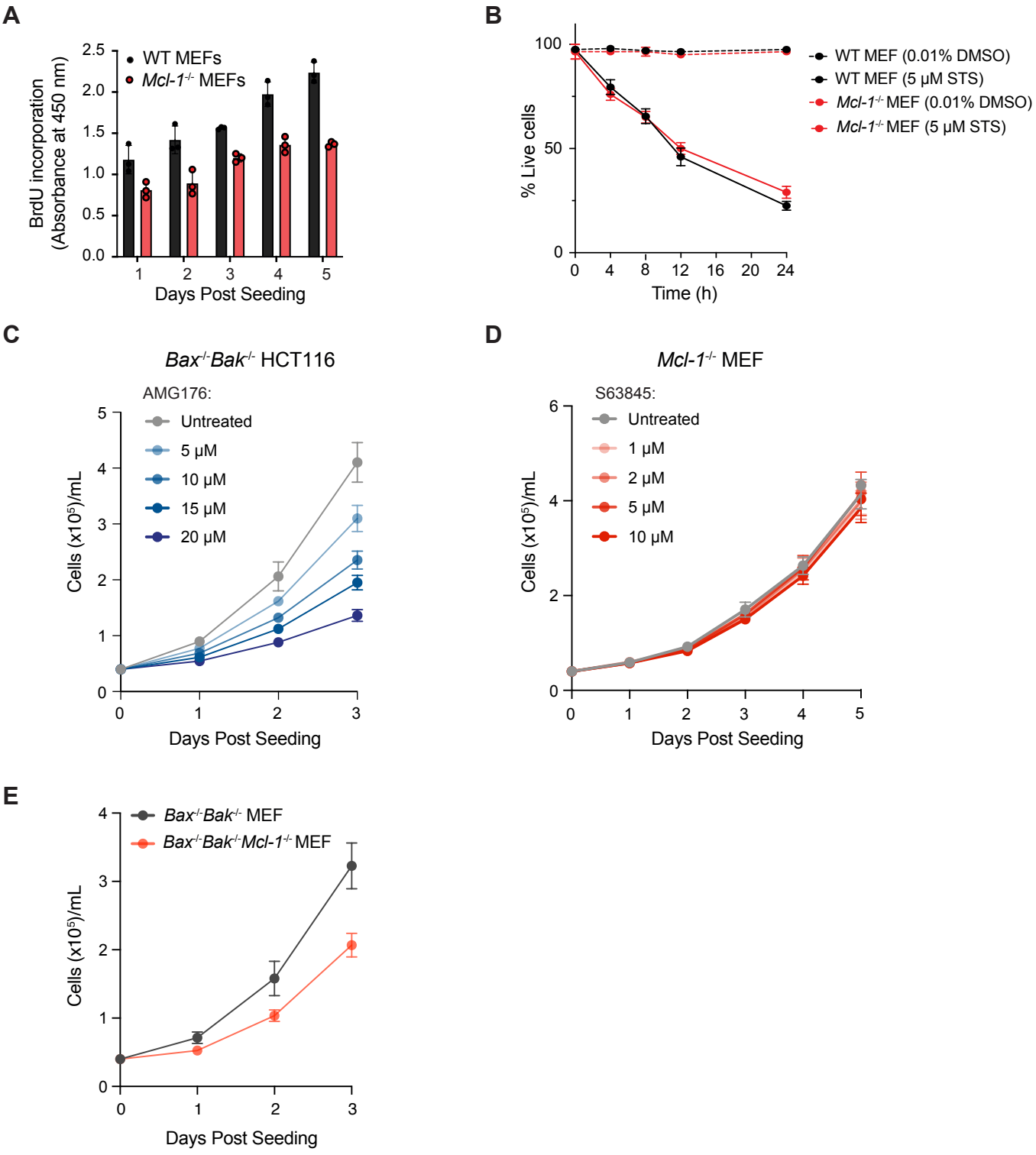

Adhikary et al. Figure S1

Figure S1, Related to Figure 1. Proliferation and Viability of Cell Lines with Discrete Genetic Lesions Over Time and in Response to Drug Treatments.

(A) Measurement of WT and *Mcl-1*$^{-/-}$ MEF cell proliferation at days 1-5 post seeding as assessed by BrdU assay. Data are mean ± S.D. for experiments performed in technical triplicate and conducted twice with similar results.

(B) Measurement of percent viability of WT and *Mcl-1*$^{-/-}$ MEFs by trypan blue staining detected cell death induced by staurosporine at 4, 8, 12, and 24 hours post-treatment, whereas vehicle-treated cells maintained 100% viability. Data are mean ± S.D. for experiments performed in technical duplicate and conducted twice using independent preparations of cells and drug, with similar results.

(C) Pharmacologic blockade of MCL-1 by AMG176 for 72 hours caused a dose-responsive decrease in cell proliferation of *Bax*$^{-/-}$*Bak*$^{-/-}$ HCT116 cells compared to untreated cells, as measured by trypan blue staining and cell count. Data are mean ± S.D. for experiments performed in technical duplicate and conducted twice using independent preparations of cells and drug with similar results.

(D) Treatment of *Mcl-1*$^{-/-}$ MEFs with S63845 had no effect on cell proliferation compared to untreated cells, as measured by trypan blue staining and cell count through day 5 post seeding. Data are mean ± S.D. for experiments performed in technical duplicate and conducted twice using independent preparations of cells and drug, with similar results.

(E) Comparative cell proliferation of *Bax*$^{-/-}$*Bak*$^{-/-}$ (DKO) and *Mcl-1*$^{-/-}$*Bax*$^{-/-}$*Bak*$^{-/-}$ (TKO) MEFs as measured by trypan blue staining and cell count at days 0-3 post seeding. Data are mean ± S.D. for experiments performed in technical triplicate and conducted twice using independent preparations of cells.

A

MEF

Cell Viability (%)

Days post seeding	WT	*Mcl-1*$^{-/-}$
0	96.5 ± 0.7	98.5 ± 0.7
1	98.5 ± 0.7	95.0 ± 0
2	94.5 ± 0.7	95.5 ± 2.1
3	98.0 ± 0	97.5 ± 2.1

B

MEF

Cell Viability (%)

Days post seeding	*Mcl-1*$^{fl/fl}$Rosa-CreER^{T2}	*Mcl-1*$^{fl/fl}$Rosa-CreER^{T2} + TAM	*Mcl-1*$^{fl/fl}$Rosa-CreER^{T2} + TAM + MCL-1
0	93.5 ± 0.7	96.5 ± 2.1	99.0 ± 0
1	94.5 ± 3.5	97.5 ± 0.7	97.0 ± 1.4
2	95.0 ± 0	94.5 ± 0.7	96.0 ± 1.4
3	93.0 ± 1.4	96.5 ± 0.7	97.5 ± 0.7

C

MEF

Cell Viability (%)

Days post seeding	*Mcl-1*$^{fl/fl}$Rosa-CreER^{T2} + TAM	*Mcl-1*$^{fl/fl}$Rosa-CreER^{T2} + TAM + MCL-1^{Matrix}	*Mcl-1*$^{fl/fl}$Rosa-CreER^{T2} + TAM + MCL-1^{OMM}
0	94.5 ± 0.7	92.5 ± 0.7	97.0 ± 2.8
1	97.5 ± 0.7	94.0 ± 0	96.0 ± 0
2	95.0 ± 1.4	94.0 ± 1.4	97.5 ± 0.7
3	96.0 ± 1.4	95.0 ± 2.8	97.0 ± 1.4

D

Bax$^{-/-}$*Bak*$^{-/-}$ MEF

S63845 (μM)	Cell Viability (%)
0	98.5 ± 0.7
5	97.5 ± 0.7
10	96.5 ± 0.7
15	97.5 ± 0.7
20	95.5 ± 0.7

E

Bax$^{-/-}$*Bak*$^{-/-}$ MEF

AMG176 (μM)	Cell Viability (%)
0	94.5 ± 3.5
5	98.0 ± 2.8
10	96.5 ± 2.1
15	98.5 ± 2.1
20	95.0 ± 1.4

F

Bax$^{-/-}$*Bak*$^{-/-}$ HCT116

AMG176 (μM)	Cell Viability (%)
0	95.0 ± 2.8
5	94.5 ± 0.7
10	96.5 ± 2.1
15	97.5 ± 0.7
20	98.0 ± 2.8

G

Bax$^{-/-}$*Bak*$^{-/-}$ MEF

ABT199 (μM)	Cell Viability (%)
0	93.0 ± 1.4
5	92.5 ± 3.5
10	95.5 ± 0.7
15	97.0 ± 2.8
20	95.0 ± 2.8

H

Bax$^{-/-}$*Bak*$^{-/-}$ HCT116

S63845 (μM)	Cell Viability (%)
0	98.0 ± 1.4
5	94.0 ± 2.8
10	95.0 ± 0
15	95.5 ± 2.1
20	93.0 ± 1.4

I

Bax$^{-/-}$*Bak*$^{-/-}$ MV4;11

S63845 (μM)	Cell Viability (%)
0	95.0 ± 4.2
5	92.5 ± 3.5
10	94.0 ± 1.4
15	99.5 ± 0.7
20	96.5 ± 4.9

J

WT MEF

S63845 (μM)	Cell Viability (%)
0	97.5 ± 0.7
1	97.5 ± 2.1
2	96.5 ± 0.7
5	93.5 ± 0.7
10	89.0 ± 1.4

K

Mcl-1$^{-/-}$ MEF

S63845 (μM)	Cell Viability (%)
0	98.0 ± 1.4
1	97.5 ± 0.7
2	95.5 ± 0.7
5	97.5 ± 0.7
10	95.5 ± 0.7

L

Bax$^{-/-}$*Bak*$^{-/-}$ MEF

Days post seeding	Cell Viability (%)
0	95.5 ± 4.2
1	95.0 ± 1.4
2	94.0 ± 0.0
3	96.5 ± 2.1

M

Bax$^{-/-}$*Bak*$^{-/-}$*Mcl-1*$^{-/-}$ MEF

Days post seeding	Cell Viability (%)
0	96.5 ± 0.7
1	96.5 ± 3.5
2	94.0 ± 1.4
3	95.5 ± 0.7

N

Bax$^{-/-}$*Bak*$^{-/-}$ MEF

Treatment	Cell Viability (%)
Vehicle	96.5 ± 2.5
S63845 (10 μM)	96.5 ± 0.6
Vincristine (10 nM)	96.5 ± 0.7
Co-treatment	94.0 ± 2.5

Figure S2, Related to Figures 1 and 4D. Viability of Cell Lines with Discrete Genetic Deletions and in Response to Drug Treatments.

(A-N) Percent viability was measured by trypan blue staining and cell count of (A) wild-type and *Mcl-1*$^{-/-}$ MEFs at days 0-3 post seeding, (B) *Mcl-1*$^{fl/fl}$Rosa-ERCre^{T2} MEFs, tamoxifen-treated *Mcl-1*$^{fl/fl}$Rosa-ERCre^{T2} MEFs, and tamoxifen-treated *Mcl-1*$^{fl/fl}$Rosa-ERCre^{T2} MEFs reconstituted with MCL-1 at days 0-3 post seeding, (C) tamoxifen-treated *Mcl-1*$^{fl/fl}$Rosa-ERCre^{T2} MEFs and those reconstituted with either MCL-1^{OMM} or MCL-1^{Matrix} at days 0-3 post seeding, (D) *Bax*$^{-/-}$*Bak*$^{-/-}$ MEFs treated with S63845 at the indicated doses for 72 hours, (E) *Bax*$^{-/-}$*Bak*$^{-/-}$ MEFs treated with AMG176 at the indicated doses for 72 hours, (F) *Bax*$^{-/-}$*Bak*$^{-/-}$ HCT116 cells treated with AMG176 at the indicated doses for 72 hours, (G) *Bax*$^{-/-}$*Bak*$^{-/-}$ MEFs treated with ABT-199 (Venetoclax) at the indicated doses for 72 hours, (H) *Bax*$^{-/-}$*Bak*$^{-/-}$ HCT116 cells treated with S63845 at the indicated doses for 72 hours, (I) *Bax*$^{-/-}$*Bak*$^{-/-}$ MV4;11 leukemia cells treated with S63845 at the indicated doses for 96 hours, (J) wild-type MEFs treated with S63845 at the indicated doses for 72 hours, (K) *Mcl-1*$^{-/-}$ MEFs treated with S63845 at the indicated doses for 72 hours, (L) *Bax*$^{-/-}$*Bak*$^{-/-}$ MEFs at days 0-3 post seeding, (M) *Mcl-1*$^{-/-}$*Bax*$^{-/-}$*Bak*$^{-/-}$ (TKO) MEFs at days 0-3 post seeding, and (N) *Bax*$^{-/-}$*Bak*$^{-/-}$ MEFs treated with vehicle (0.5% DMSO), vincristine, S63845, or the combination at the indicated doses for 16 hours. Data are mean ± S.D. for experiments performed in technical duplicate and conducted twice using independent preparations of cells and drug treatments, where indicated, with similar results.

A

Drug	Mechanism of Action	Correlation
BRD-K70511574	Plk1 inhibitor	0.782
nakiterpiosin	Impairs spindle assembly	0.761
tivantinib	RTK inhibitor (cMet); Anti-mitotic	0.759
FQI-1	Anti-proliferative/Anti-mitotic	0.755
ceranib-2	Ceramidase inhibitor	0.741
FQI-2	Anti-proliferative/Anti-mitotic	0.741
parbendazole	Anti-helminthic/Anti-mitotic	0.731
triazolothiadiazine	Anti-mitotic	0.726
GSK461364	Plk1 inhibitor	0.712
rigosertib	Ras inhibitor; Anti-mitotic	0.709
YK-4-279	ETV1 inhibitor; Anti-mitotic	0.709
GW-843682X	PLK1 inhibitor	0.689
evodiamine	Anti-inflammatory	0.688
paclitaxel	Anti-mitotic	0.68
NVP-231	Ceramide kinase inhibitor	0.679
narciclasine	Anti-inflammatory	0.667
LY2183240	FAAH inhibitor	0.667
KX2-391	Src-kinase inhibitor; Anti-mitotic	0.661
CHM-1	Anti-mitotic	0.656
SB-225002	CXCR2 antagonist/Anti-mitotic	0.653
teniposide	Topoisomerase II inhibitor	0.652
docetaxel	Anti-mitotic	0.648
BI-2536	Plk1 inhibitor	0.643
SB-743921	Eg5 inhibitor	0.637
tipifarnib	Farnesyltransferase inhibitor	0.635
BRD9876:MK-1775	Anti-mitotic/Wee1 inhibitor	0.633
gemcitabine	DNA synthesis inhibitor	0.628
cytarabine	DNA polymerase inhibitor	0.626
PHA-793887	Pan-CDK inhibitor	0.625
PL-DI	ROS inducer	0.624
etoposide	Topoisomerase II inhibitor	0.621
docetaxel:tanespimycin	Anti-mitotic/HSP90 inhibitor	0.621
KPT-185	XPO1 inhibitor/Anti-proliferative	0.621
clofarabine	DNA synthesis inhibitor	0.62
vorinostat	HDAC inhibitor/Anti-proliferative	0.619
SR-II-138A	Translation inhibitor	0.618
doxorubicin	Topoisomerase II inhibitor	0.613
pevonedistat	Nedd8 activating enzyme inhibitor	0.612
carboplatin:etoposide	Topoisomerase II inhibitor	0.609
topotecan	Topoisomerase II inhibitor	0.608
alisertib	Aurora kinase A/B inhibitor	0.608
CD-437	Retinoic acid gamma receptor agonist	0.603
BRD-K34222889	ROS inducer	0.601
PF-03758309	PAK4 inhibitor/Anti-proliferative	0.598
PF-184	IKK2 inhibitor	0.597
MK-1775	Wee1 inhibitor	0.596

B

Drug	Mechanism of Action	Correlation
bitopertin	Glycine reuptake inhibitor	0.47499
brivaracetam	Anti-convulsant	0.44143
KG-5	B-Raf inhibitor	0.46253
pardoprunox	Dopamine receptor agonist	0.43394
PHA-793887	Pan-CDK inhibitor	0.41639
methiazole	Anti-helminthic/Anti-mitotic	0.41304
benzethonium	Anti-septic/Anti-bacterial	0.40997
ARQ-621	Kinesin inhibitor	0.43467
SB-743921	Eg5 inhibitor	0.40812
SB-225002	CXCR2 antagonist/Anti-mitotic	0.40787
mebendazole	Anti-helminthic/Anti-mitotic	0.40187
litronesib	Eg5 inhibitor	0.40573
tivantinib	RTK inhibitor (cMet); Anti-mitotic	0.39886
D-64131	Anti-mitotic	0.39453
octenidine	Anti-septic	0.39552
uprosertib	Akt inhibitor	0.39471
OSI-930	c-Kit inhibitor	0.4036
BMS-754807	IGF-1R inhibitor	0.39057
xanomeline	Acetylcholine receptor agonist	0.38884
KF-38789	P-selectin-mediated-cell adhesion inhibitor	0.38679
tozasertib	Pan-Aurora kinase inhibitor	0.38494
SNS-314	Pan-Aurora kinase inhibitor	0.3859
PF-03758309	PAK4 inhibitor/Anti-proliferative	0.38372
oxiracetam	Central nervous system stimulant	0.3826
BML-284	Wnt agonist	0.40532
alexidine	Anti-microbial	0.38139
10-deacetylbaccatin	Anti-mitotic	0.3883
YK-4-279	ETV1 inhibitor; Anti-mitotic	0.40276
CUDC-101	HDAC inhibitor	0.37637
CMPD-1	MK2 inhibitor/Anti-mitotic	0.37514
PHA-680632	Pan-Aurora kinase inhibitor	0.37329
thiostrepton	Anti-microbial	0.37318
crizotinib	ALK and ROS1 inhibitor	0.37154
MLN-8054	Aurora kinase A inhibitor	0.3784
alisertib	Aurora kinase A/B inhibitor	0.37259
AZ3146	MPS1 kinase inhibitor/Anti-mitotic	0.36896
ispinesib	KSP kinase inhibitor/Anti-mitotic	0.36949
oxyphencyclimine	Muscarinic receptor antagonist	0.37434
entinostat	HDAC inhibitor	0.36794
NVP-231	Ceramide kinase inhibitor	0.39213
CCT129202	Aurora kinase A inhibitor	0.36756
GW-843682X	PLK1 inhibitor	0.36674
4SC-202	HDAC inhibitor	0.38828
CYC116	Aurora kinase A/B inhibitor	0.3642
resminostat	HDAC inhibitor	0.36327
TH-302	Hypoxia activated prodrug	0.36243
vinflunine	Anti-mitotic	0.3844

C

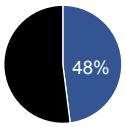

ML311 (CTRP v2)

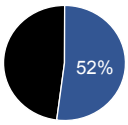

S63845 (PRISM)

Mechanism of Action	# of Drugs within Top 75	
	CTRP v2	PRISM
Anti-proliferative/Anti-mitotic (PLK1, KSP, Eg5, CDK inhibitors)	19	21
DNA Damaging Agent	9	2
Microtubule Targeting Agent	5	6
Aurora Kinase Inhibitor	3	10

D

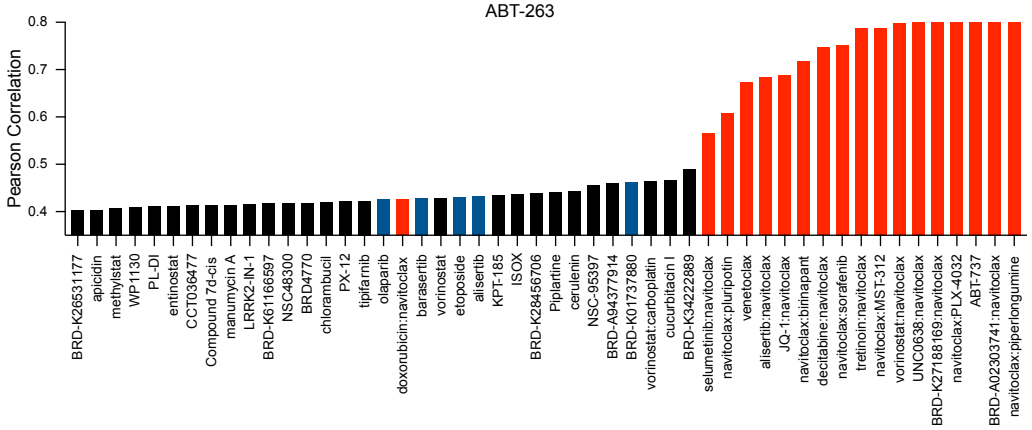

E

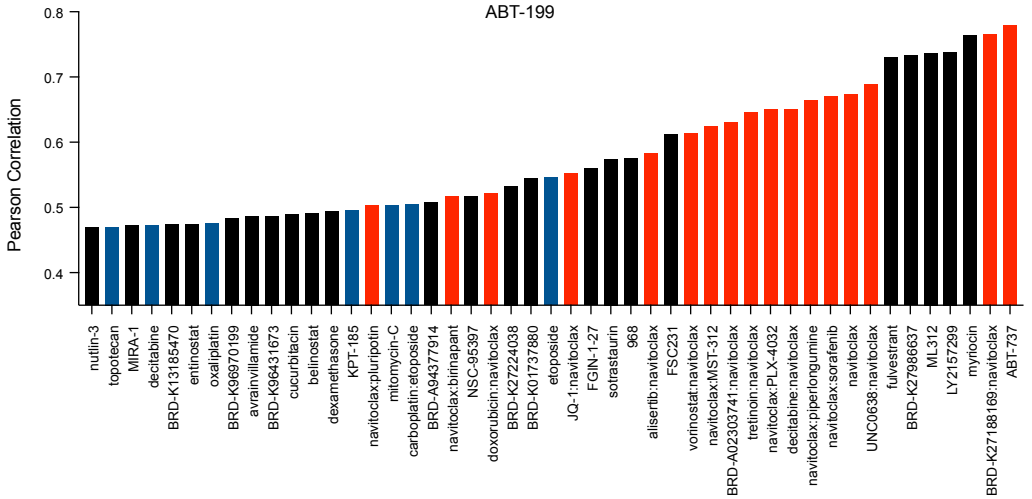

Adhikary et al. Figure S3

Figure S3, Related to Figure 2. Ranked Listings of Drugs whose Pharmacologic Profiles Correlate with Treatment by Inhibitors of Select BCL-2 Family Anti-Apoptotic Proteins.

(A) Ranked list of drugs that correlate most with ML311 pharmacologic activity across cancer cell lines in the CTRP v2 dataset (Fig 2D). The targets and/or mechanisms of action for each drug, and the correlation coefficients, are shown. Drug names colored in blue are common to those identified for the distinct S63845 analysis in B.

(B) Ranked list of drugs within the Drug Repurposing Hub dataset (Broad Institute) that correlate most with S63845 pharmacologic activity across the CCLE. The targets and/or mechanisms of action for each drug, and the correlation coefficients, are shown. Drug names colored in blue are common to those identified for the distinct ML311 analysis in A.

(C) Fifty percent of the top 75 drugs that correlate with ML311 or S63845 activity across the CCLE harbor common mechanisms of action as anti-proliferative/anti-mitotic drugs, DNA damaging agents, microtubule targeting agents, or aurora kinase inhibitors.

(D-E) Treatment with Navitoclax (ABT-263; BCL-2/BCL-X_L inhibitor) (D) or Venetoclax (ABT-199; selective BCL-2 inhibitor) (E) correlates with the pharmacologic profiles of apoptosis-inducing drugs or their respective drug combinations, as demonstrated by analyzing the sensitivity data for 500 drugs across the CCLE (CTRP v2, Broad Institute). Molecular modulators of the apoptotic pathway are colored red, and anti-proliferative and anti-mitotic compounds are colored blue.

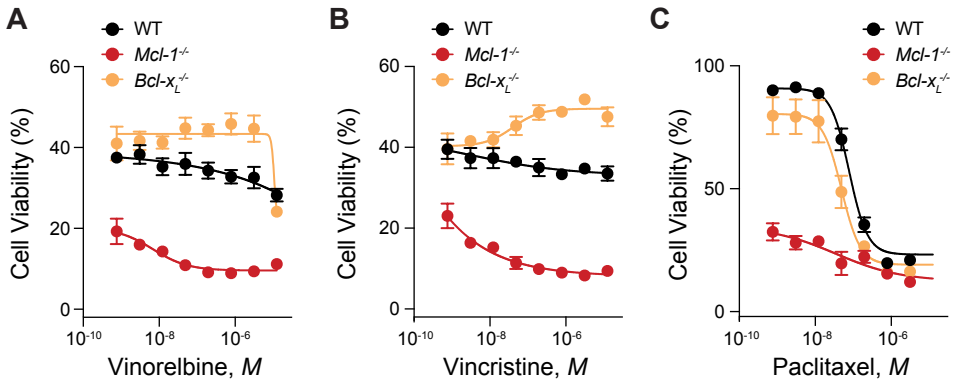

Adhikary et al. Figure S4

Figure S4, Related to Figure 3. Relative Susceptibility of Wild-Type, *Mcl-1*$^{-/-}$, and *Bcl-x*$_L$$^{-/-}$ MEFs to Treatment with Vinorelbine, Vincristine, or Paclitaxel.

(A-C) Deletion of *Mcl-1*$^{-/-}$ but not *Bcl-x*$_L$$^{-/-}$ sensitizes MEFs to the microtubule targeting agents (MTAs) vinorelbine (A), vincristine (B), and paclitaxel (C). Data are mean ± S.D. for experiments performed in technical triplicate and conducted twice using independent preparations of cells and MTAs with similar results.

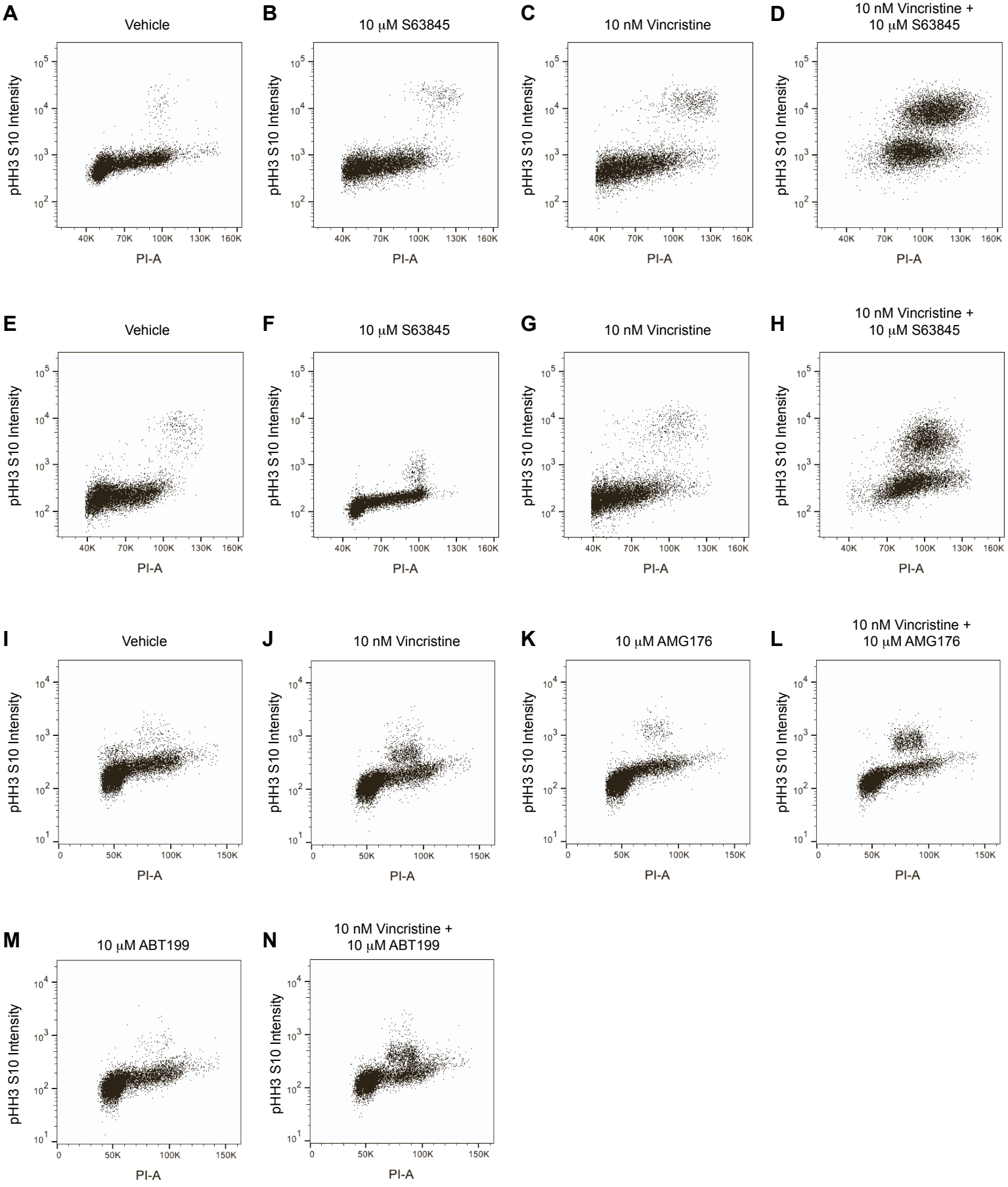

Adhikary et al. Figure S5

Figure S5, Related to Figures 4 and S6. FACS-based Cell Cycle Analyses of Drug-treated WT MEF, *Bax*$^{-/-}$*Bak*$^{-/-}$ MEF, and *Bax*$^{-/-}$*Bak*$^{-/-}$ HCT116 Cells.

(A-D) Representative cell cycle scatter plots showing phospho-histone H3 (pHH3) S10 vs. propidium iodide (PI) staining intensities in WT MEFs treated with vehicle (0.1% DMSO) (A), 10 μM S63845 (B), 10 nM vincristine (C), or the combination of 10 μM S63845 and 10 nM vincristine (D). Cells in mitosis show higher (pHH3) S10 intensity and higher DNA content, as assessed by PI staining. Plots were generated after gating on singlet cells only.

(E-H) Representative cell cycle scatter plots showing phospho-histone H3 (pHH3) S10 vs. propidium iodide (PI) staining intensities in *Bax*$^{-/-}$*Bak*$^{-/-}$ MEFs treated with vehicle (0.1% DMSO) (E), 10 μM S63845 (F), 10 nM vincristine (G), or the combination of 10 μM S63845 and 10 nM vincristine (H). Cells in mitosis show higher (pHH3) S10 intensity and higher DNA content, as assessed by PI staining. Plots were generated after gating on singlet cells only.

(I-N) Representative cell cycle scatter plots showing phospho-histone H3 (pHH3) S10 vs. propidium iodide (PI) staining intensities in *Bax*$^{-/-}$*Bak*$^{-/-}$ HCT116 cells treated with vehicle (0.1% DMSO) (I), 10 nM vincristine (J), 10 μM AMG176 (K), the combination of 10 μM AMG176 and 10 nM vincristine (L), 10 μM ABT-199 (Venetoclax) (M), the combination of 10 μM ABT-199 (Venetoclax) and 10 nM vincristine (N). Cells in mitosis show higher (pHH3) S10 intensity and higher DNA content, as assessed by PI staining. Plots were generated after gating on singlet cells only.

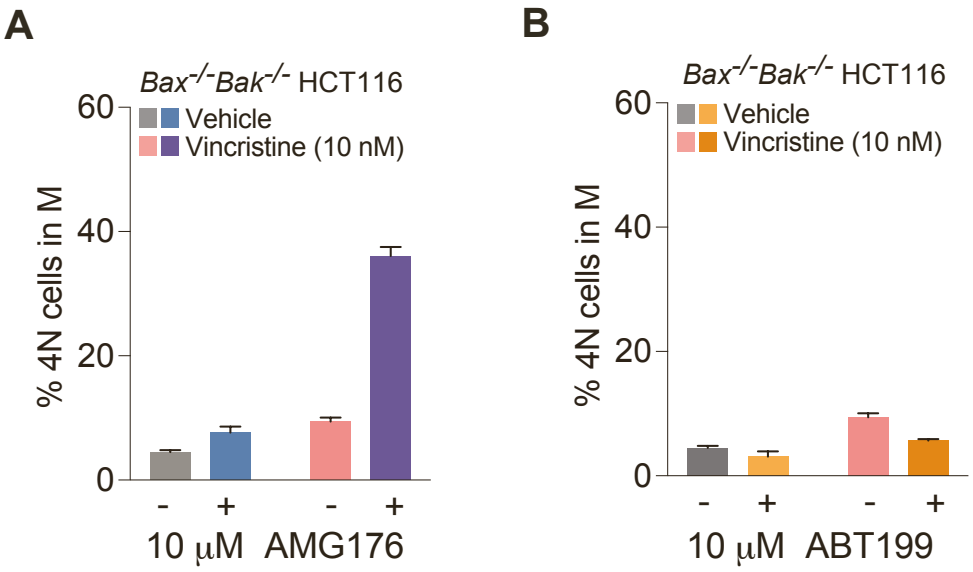

Adhikary et al. Figure S6

Figure S6, Related to Figure 4. Cell Cycle Effects of AMG176 and Venetoclax Treatment of *Bax*$^{-/-}$*Bak*$^{-/-}$ HCT116 Cells.

(A-B) Combination treatment with AMG176 and vincristine for 16 hours caused mitotic arrest in *Bax*$^{-/-}$*Bak*$^{-/-}$ HCT116 cells (A), whereas combination treatment with ABT-199 (Venetoclax) and vincristine had no such effect (B). Data are mean ± S.D. for experiments performed in technical duplicate and conducted twice using independent preparations of cells and drugs with similar results.

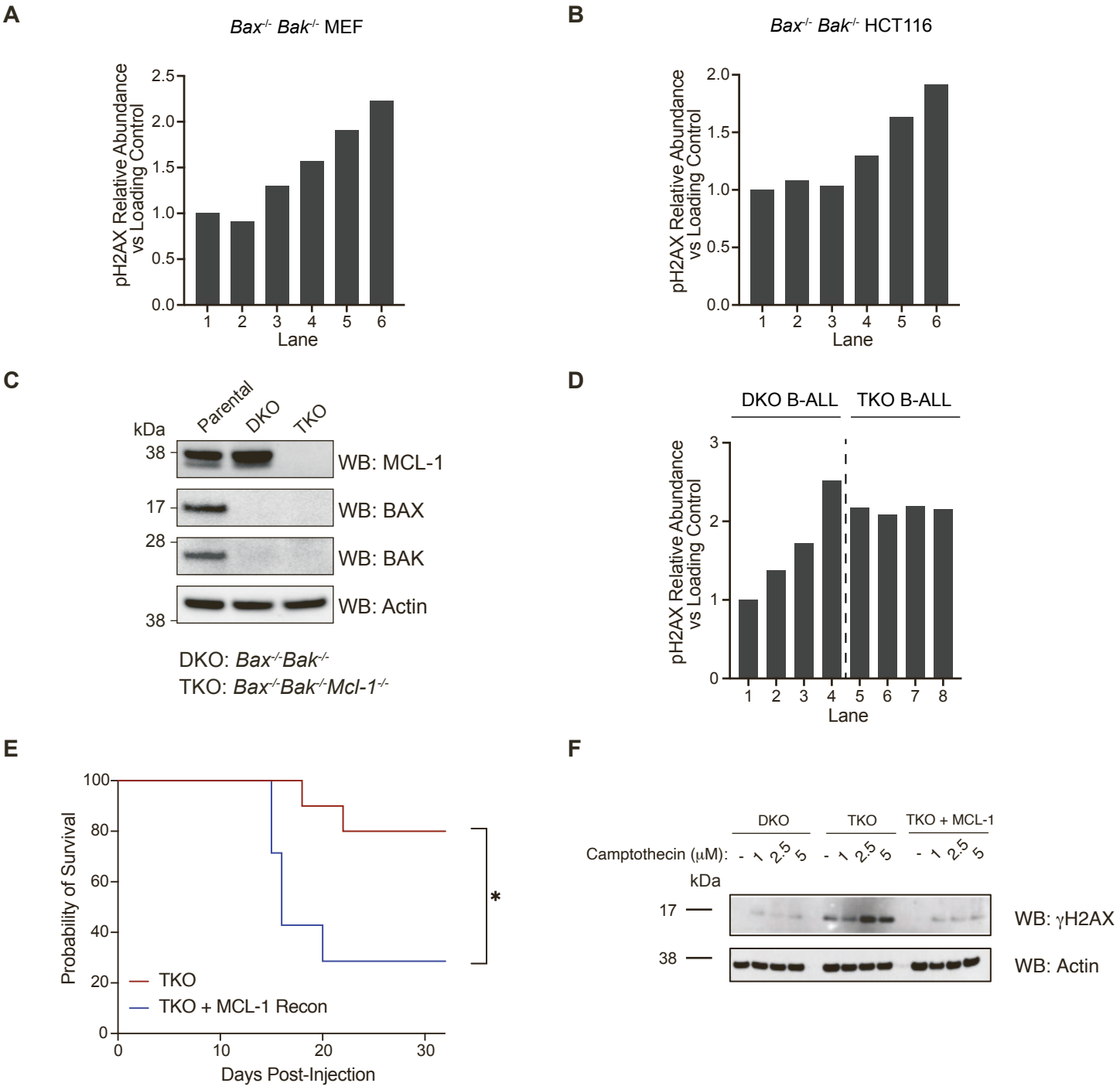

Adhikary et al. Figure S7

Figure S7, Related to Figures 5 and 6. Quantitation of S63845-induced DNA Damage in DKO and TKO Cells, and Rescue of TKO Phenotype upon MCL-1 Reconstitution.

(A-B) Quantitation of γH2AX levels in response to S63845 treatment of *Bax*$^{-/-}$*Bak*$^{-/-}$ MEFs (A) and *Bax*$^{-/-}$*Bak*$^{-/-}$ HCT116 cells (B), as measured by densitometry of western blots (Figures 5G and 5H, respectively).

(C) Western analyses of MCL-1, BAX, BAK, and actin in parental, *Bax*$^{-/-}$*Bak*$^{-/-}$ (DKO) and *Mcl-1*$^{-/-}$*Bax*$^{-/-}$*Bak*$^{-/-}$ (TKO) B-ALL cells.

(D) Quantitation of γH2AX levels in response to S63845 treatment of *Bax*$^{-/-}$*Bak*$^{-/-}$ (DKO) and *Mcl-1*$^{-/-}$*Bax*$^{-/-}$*Bak*$^{-/-}$ (TKO) B-ALL cells, as measured by densitometry of the western blot (Figures 5I).

(E) Reconstitution of TKO B-ALL cells with hMCL-1 restored the high engraftment rate of DKO cells as compared to TKO cells, as monitored for 33 days in mice administered 500,000 leukemic cells by tail vein (n=10 mice per arm; *, p=0.013).

(F) The increased susceptibility of TKO B-ALL cells to DNA damage induced by 24 hour camptothecin treatment, relative to DKO B-ALL cells, is rescued by reconstitution of TKO B-ALL cells with MCL-1, as assessed by γH2AX western analysis.

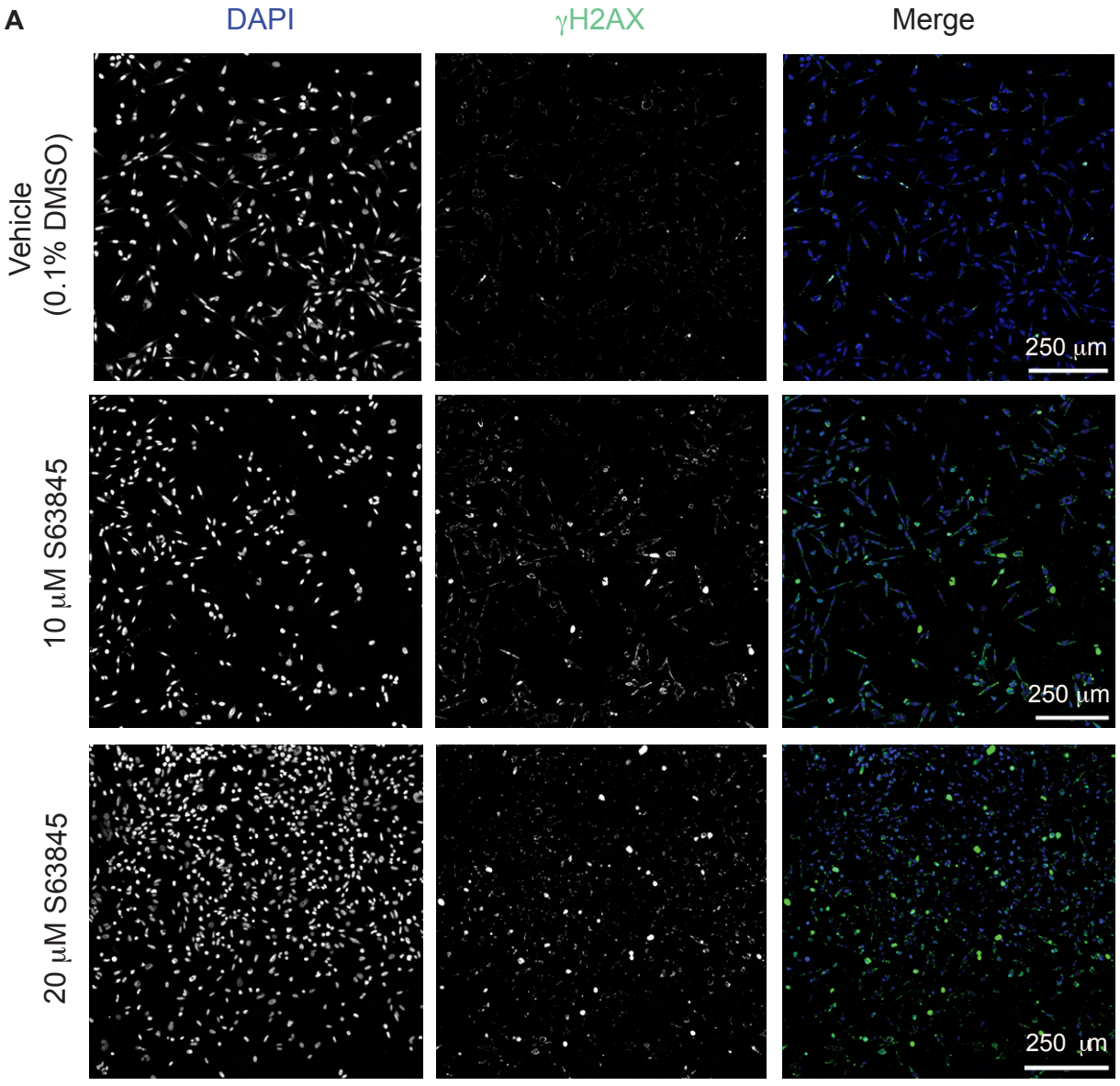

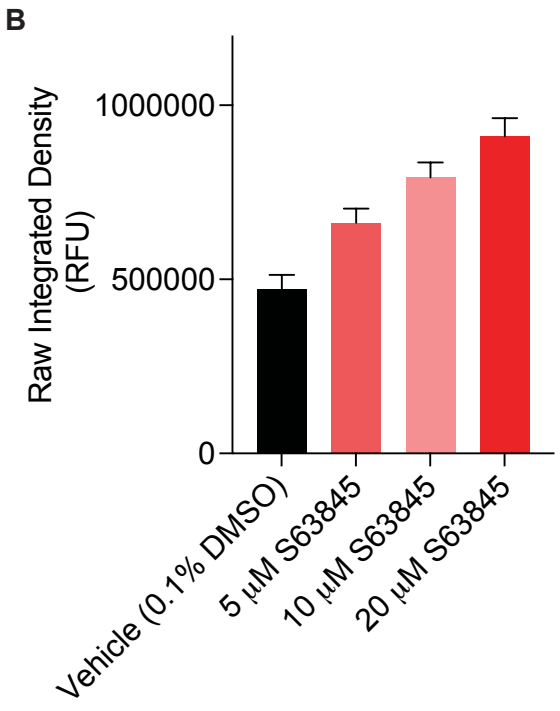

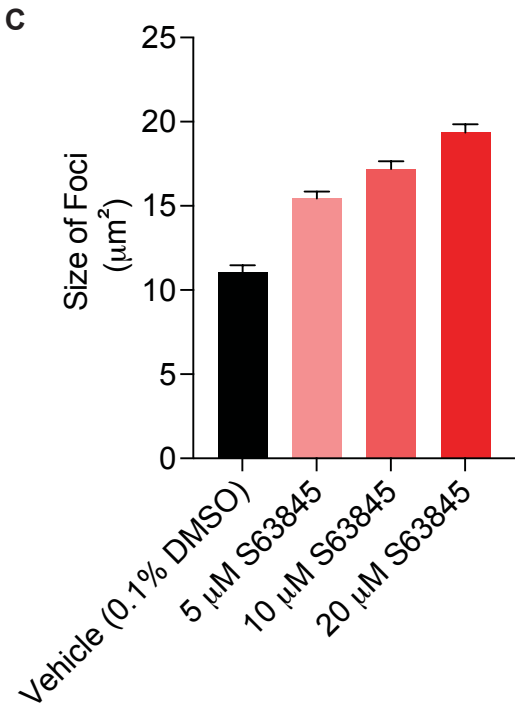

Adhikary et al. Figure S8

Figure S8, Related to Figure 5. Detection and Quantitation of DNA Damage Nuclear Foci in S63845-treated Cells.

(A) *Bax*$^{-/-}$*Bak*$^{-/-}$ MEFs were treated with vehicle (top row) or the indicated doses of S63845 (middle and bottom row) and subjected to DAPI staining (left column), immunofluorescence detection of γH2AX (middle column), and overlay of the microscopy images (right column).

(B-C) Raw integrated density (B) and the size of nuclear foci (C) were quantitated by ImageJ analysis. RFU, relative fluorescence units. Data are mean ± S.E.M. for experiments performed in technical triplicate.

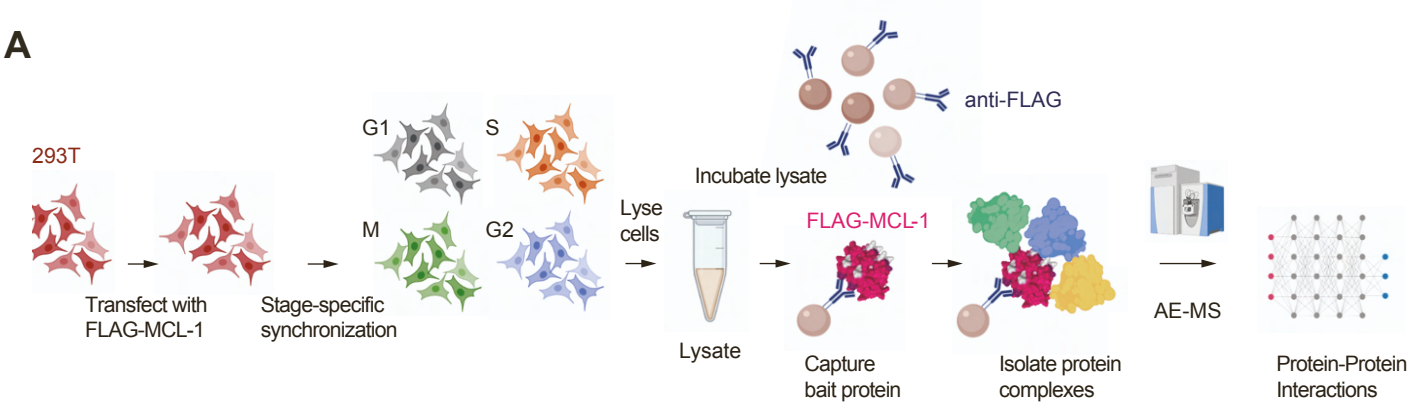

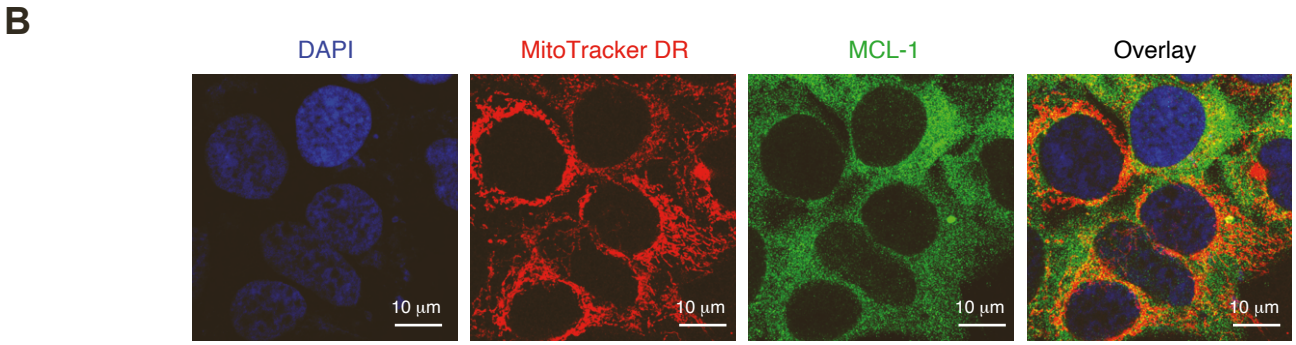

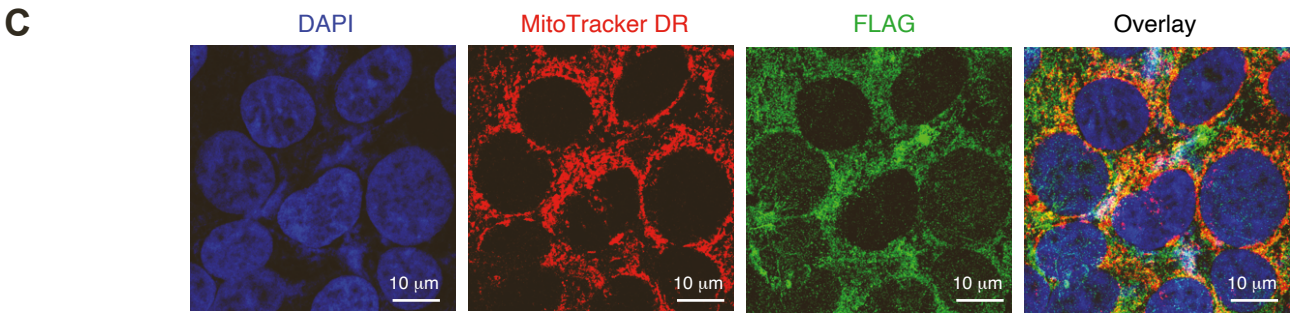

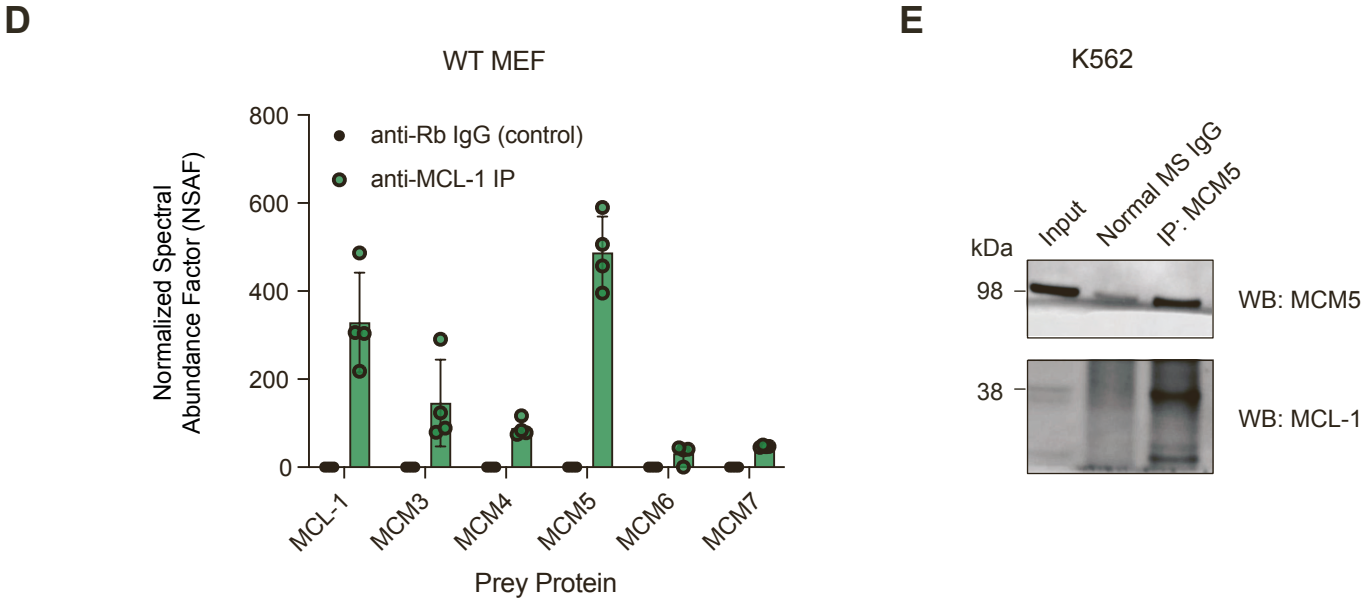

Adhikary et al. Figure S9

Figure S9, Related to Figure 7. AE-MS Workflow, Immunolocalization of Endogenous and FLAG-tagged MCL-1 in Cells, and Validation of the Interaction Between MCL-1 and Members of the MCM Complex.

(A) Affinity enrichment mass spectrometry (AE-MS) workflow for capture of FLAG-MCL-1 bound proteins in lysates from HEK 293T cells at each stage of the cell cycle.

(B-C) Immunofluorescence imaging of endogenous MCL-1 in untransfected 293T cells (B) and FLAG in FLAG-MCL-1 transfected 293T cells (C) (green). Cells were counterstained with the nuclear marker DAPI (blue) and the mitochondrial marker MitoTracker DR (red).

(D) Enrichment of MCM complex members in MCL-1 immunoprecipitates from wild-type MEF lysates, as detected by AP-MS using anti-MCL-1 (green) and control anti-rabbit IgG (black) antibodies. The normalized spectral abundance factor (NSAF) values for MCM complex members 3-7 are shown. Four biological replicates of the AP-MS experiments were performed.

(E) Co-immunoprecipitation of native MCL-1 and MCM5 from lysates of MCL-1 independent K562 cells using an MCL-1 antibody.

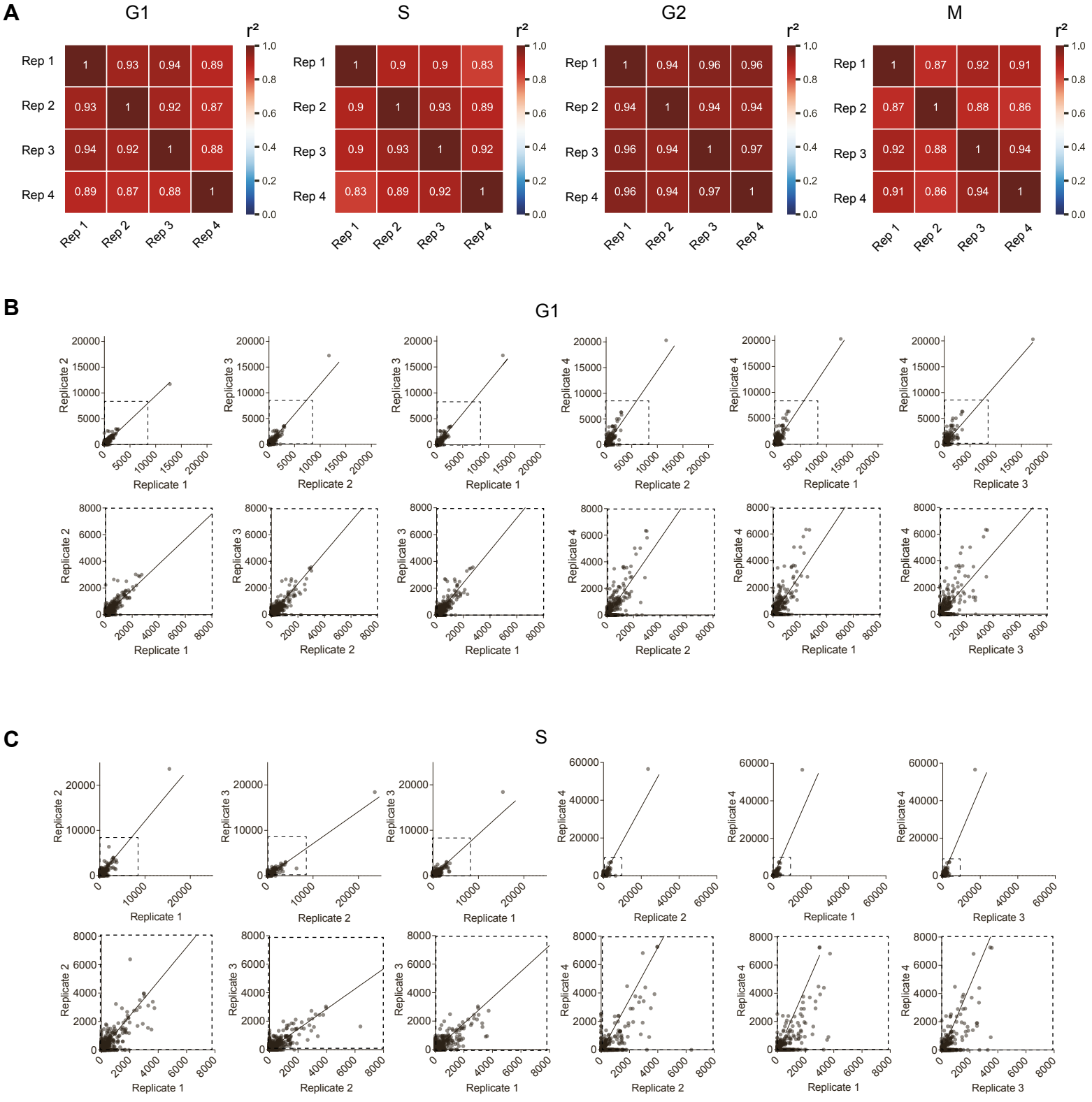

Adhikary et al. Figure S10

D

G2

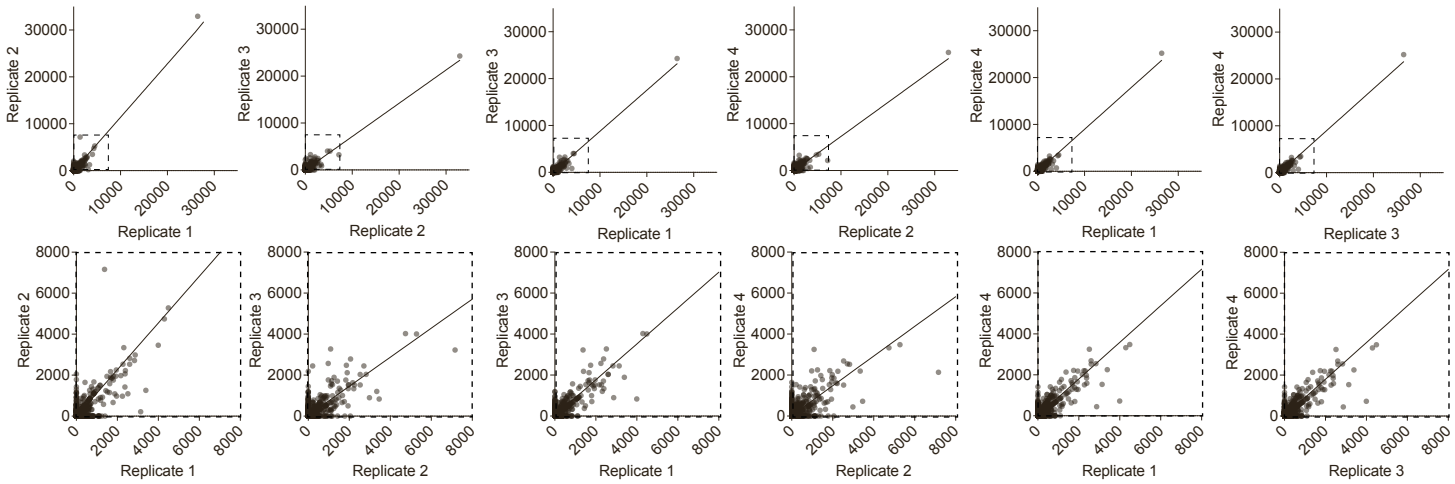
Replicate 2
Replicate 1
Replicate 3
Replicate 2
Replicate 3
Replicate 1
Replicate 4
Replicate 2
Replicate 4
Replicate 1
Replicate 4
Replicate 3
0
10000
20000
30000
2000
4000
6000
8000

E

M

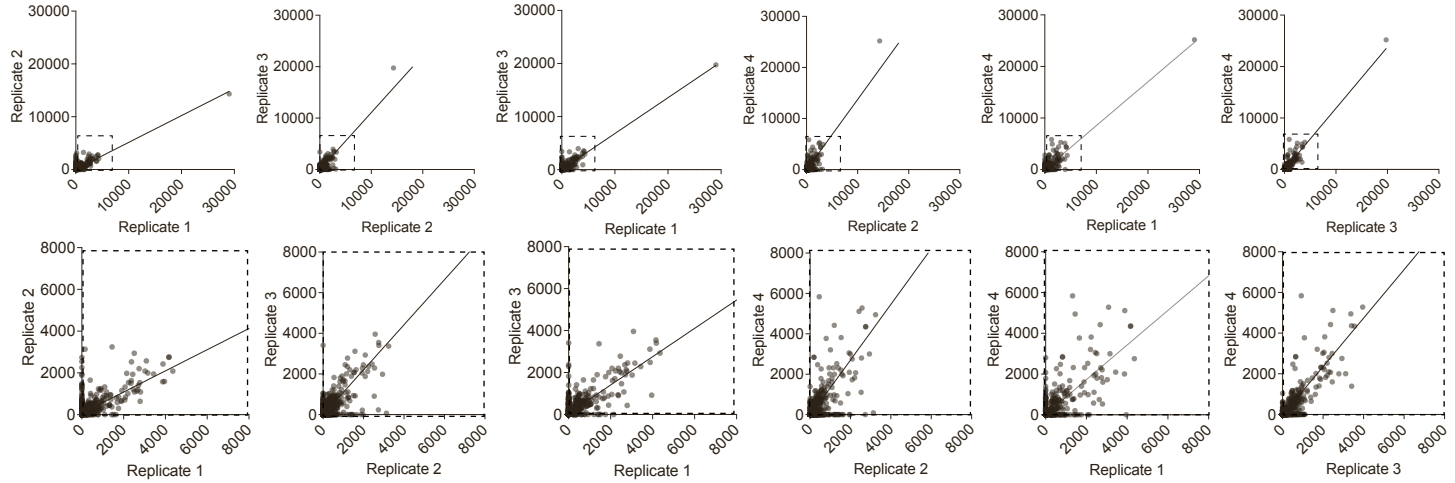
Replicate 2
Replicate 1
Replicate 3
Replicate 2
Replicate 3
Replicate 1
Replicate 4
Replicate 2
Replicate 4
Replicate 1
Replicate 4
Replicate 3
0
10000
20000
30000
2000
4000
6000
8000

Figure S10, Related to Figure 7. Replicates of AE-MS Across Each Stage of the Cell Cycle.

(A) Summary table of Pearson correlations for biological replicates (n=4) of the AE-MS analyses of anti-FLAG immunoprecipitates from lysates of FLAG-MCL-1 expressing HEK293T cells.

(B-E) Pairwise scatter plots of normalized spectral abundance factors (NSAFs) for the identified proteins among biological replicates performed at the G1 (B), S (C), G2 (D), and M (E) stages of the cell cycle. Dashed box portion of each plot is expanded below. For all plots, statistical significance of the correlation is $p<0.0001$.

A

Uniprot ID	Protein	Unique Peptides	Razor Peptides	G1 Phase Abundance	S Phase Abundance	G2 Phase Abundance	M Phase Abundance	G1 Phase Rank	S Phase Rank	G2 Phase Rank	M Phase Rank
Q07820	MCL-1	580	1980	12249.95	19496.75	29699.8	21674.2	1	1	1	1
Q07812-2	BAX	0	47	932.708	325.167	0	2064.295	12	27	N/A	11
Q16611	BAK	1	24	287.817	167.977	890.915	0	88	65	>200	N/A
P12004	PCNA	65	0	470.5275	699.283	1089.822	402.6865	68	42	24	48
P06493	CDK1	0	165	1587.33	990.3695	2402.625	2576.835	6	49	2	4

B

G1 Phase

Rank	CORUM Complex Term	P-value	Odds Ratio	Combined Enrichment Score
1	F1F0-ATP synthase (EC 3.6.3.14), mitochondrial (human)	0.005646299	20.34358974	105.3137806
2	Emerin complex 52 (human)	0.013075293	12.58857143	54.59702323
3	ADAR1-CDK2 complex (human)	0.015142488	131.4370861	550.7543436
4	CDK2-CCNE1 complex (human)	0.015142488	131.4370861	550.7543436
5	Y14-Magoh complex (human)	0.015142488	131.4370861	550.7543436
6	ARD1-NATH complex (human)	0.015142488	131.4370861	550.7543436
7	Ubiquitin-protein-ligase (UBE2N, UBE2V2/MMS2) (human)	0.015142488	131.4370861	550.7543436
8	CDK2-CCNA2 complex (human)	0.015142488	131.4370861	550.7543436
9	SMRT-SKIP-CBF1 complex (human)	0.022628121	65.71523179	248.9662195
10	PGAM5-KEAP1-NRF2 complex (human)	0.022628121	65.71523179	248.9662195
11	Emerin-actin-NMI complex (human)	0.022628121	65.71523179	248.9662195
12	RBP-Jkappa-RING1-KyoT2 complex (human)	0.022628121	65.71523179	248.9662195
13	CS-MAP3K7IP1-MAP3K7IP2 complex (human)	0.022628121	65.71523179	248.9662195
14	TRIKA2 protein kinase complex (TAK1, TAB1, TAB2) (human)	0.022628121	65.71523179	248.9662195
15	ARF-Mule complex (human)	0.022628121	65.71523179	248.9662195
16	Ku antigen-NARG1 complex (human)	0.022628121	65.71523179	248.9662195
17	CASK-LIN7C-APBA1 complex (human)	0.022628121	65.71523179	248.9662195
18	p27-cyclinE-CDK2 complex (human)	0.022628121	65.71523179	248.9662195
19	CALM1-FKBP38-BCL2 complex (human)	0.022628121	65.71523179	248.9662195
20	CDC2-CCNA2-CDK2 complex (human)	0.022628121	65.71523179	248.9662195

S Phase

Rank	CORUM Complex Term	P-value	Odds Ratio	Combined Enrichment Score
1	MCM complex (human)	1.03E-04	195.5196078	1795.688136
2	Sulphiredoxin-peroxiredoxin complex (human)	0.00529304	383.5769231	2010.465718
3	snRNP-free U1A (SF-A) complex (human)	0.010558622	127.8461538	581.8038737
4	hNURF complex (human)	0.010558622	127.8461538	581.8038737
5	DCS complex (Ptbp1, Ptbp2, Hnrph1, Hnrpf) (mouse)	0.010558622	127.8461538	581.8038737
6	TNF-alpha/NF-kappa B signaling complex 9 (human)	0.013181152	95.87980769	415.0605599
7	Polycomb repressive complex 2 (PRC2) (human)	0.013181152	95.87980769	415.0605599
8	MTA1-HDAC core complex (human)	0.013181152	95.87980769	415.0605599
9	WIP-WASp-actin-myosin-IIa complex (human)	0.015796862	76.7	318.1473008
10	MTA1 complex (human)	0.015796862	76.7	318.1473008
11	TNF-alpha/NF-kappa B signaling complex 8 (human)	0.015796862	76.7	318.1473008
12	Mi2/NuRD complex (human)	0.018405771	63.91346154	255.3400953
13	SIN3 complex (human)	0.018405771	63.91346154	255.3400953
14	HDAC2-asscociated core complex (human)	0.021007896	54.78021978	211.6081512
15	Drosha complex (mouse)	0.021007896	54.78021978	211.6081512
16	Emerin complex 1 (human)	0.021007896	54.78021978	211.6081512
17	BRMS1-SIN3-HDAC complex (human)	0.021007896	54.78021978	211.6081512
18	NuRD.1 complex (human)	0.021007896	54.78021978	211.6081512
19	TNF-alpha/NF-kappa B signaling complex 7 (human)	0.021007896	54.78021978	211.6081512
20	MeCP1 complex (human)	0.023603253	47.93028846	179.5646306

G2 Phase

Rank	CORUM Complex Term	P-value	Odds Ratio	Combined Enrichment Score
1	MCM complex (human)	3.17E-04	109.3571429	881.0538514
2	Emerin complex 25 (human)	0.002460223	31.22919937	187.6095227
3	PCNA homotrimer complex (human)	0.004649936	19907	106918.5424
4	PCNA-PAF complex (human)	0.009278511	216.3695652	1012.621293
5	PCNA-p21 complex (human)	0.009278511	216.3695652	1012.621293
6	DJ-1-SNCA complex, high molecular weight complex (human)	0.009278511	216.3695652	1012.621293
7	S100A10-annexin 2 complex (mouse)	0.009278511	216.3695652	1012.621293
8	PCNA-MLH1-PMS1 complex (human)	0.0138858	108.1793478	462.6710098
9	PCNA-MSH2-MSH6 complex (human)	0.0138858	108.1793478	462.6710098
10	Emerin-actin-NMI complex (human)	0.0138858	108.1793478	462.6710098
11	PCNA-KU antigen complex (human)	0.0138858	108.1793478	462.6710098
12	Ubiquitin E3 ligase (SKP1A, SKP2, CUL1) (human)	0.0138858	108.1793478	462.6710098
13	DNMT1-G9a-PCNA complex (human)	0.0138858	108.1793478	462.6710098
14	Pre-initiation complex (PIC) (human)	0.0138858	108.1793478	462.6710098
15	Ubiquitin E3 ligase (SKP1A, FBXW2, CUL1) (human)	0.0138858	108.1793478	462.6710098
16	EXO1-MLH1-PCNA complex (human)	0.0138858	108.1793478	462.6710098
17	ING1-p300-PCNA complex (human)	0.0138858	108.1793478	462.6710098
18	PPD complex (human)	0.0138858	108.1793478	462.6710098
19	HSP90-CDC37-LRRK2 complex (human)	0.0138858	108.1793478	462.6710098
20	TRPV5-S100A10-annexin 2 complex (mouse)	0.0138858	108.1793478	462.6710098

M Phase

Rank	CORUM Complex Term	P-value	Odds Ratio	Combined Enrichment Score
1	Spliceosome (human)	3.68E-14	19.59141137	606.0266827
2	CDC5L complex (human)	4.20E-08	38.75390625	658.2146826
3	C complex spliceosome (human)	6.36E-08	17.45502646	289.244687
4	Toposome (human)	6.64E-08	203.7230769	3367.11174
5	Splicing-associated factors complex (human)	4.40E-04	100.3181818	775.3997122
6	CDC5L core complex (human)	6.57E-04	75.23484848	551.3464718
7	Nop56p-associated pre-rRNA complex (human)	6.78E-04	7.739018088	56.47120319
8	AP3 adapter complex (human)	9.15E-04	60.18484848	421.0691825
9	TREX complex (human)	0.001215037	50.15151515	336.6661399
10	Exon junction complex (human)	0.001215037	50.15151515	336.6661399
11	SF3b complex (human)	0.001215037	50.15151515	336.6661399
12	RC complex during S-phase of cell cycle (human)	0.003311249	27.34848485	156.1716008
13	RC complex during G2/M-phase of cell cycle (human)	0.003311249	27.34848485	156.1716008
14	AP3-BLOC1 complex (human)	0.004418547	23.13869464	125.4567151
15	CF IIAm complex (Cleavage factor IIAm complex) (human)	0.0050277	21.48484848	113.7148493
16	Large Drosha complex (human)	0.007822456	16.70707071	81.04193434
17	Parvulin-associated pre-rRNP complex (mouse)	0.008338889	7.688057964	36.80138985
18	DAXX-AXIN complex (human)	0.013355322	149.3609023	644.6178019
19	Daxx-Axin complex (mouse)	0.013355322	149.3609023	644.6178019
20	PSF-p54(nrb) complex (human)	0.0133553228	149.3609023	644.6178019

Adhikary et al. Figure S11

Figure S11, Related to Figure 7. Ranked Listing of Protein Complexes that Interact with MCL-1 at Each Stage of the Cell Cycle.

(A) Identification of exemplary established MCL-1 protein interactors by affinity enrichment mass spectrometry (AE-MS) across each stage of the cell cycle.

(B) Ranked listing of FLAG-MCL-1 bound protein complexes from lysates of HEK 293T cells at each stage of the cell cycle, as determined by cross-referencing AE-MS protein hits with the CORUM database.

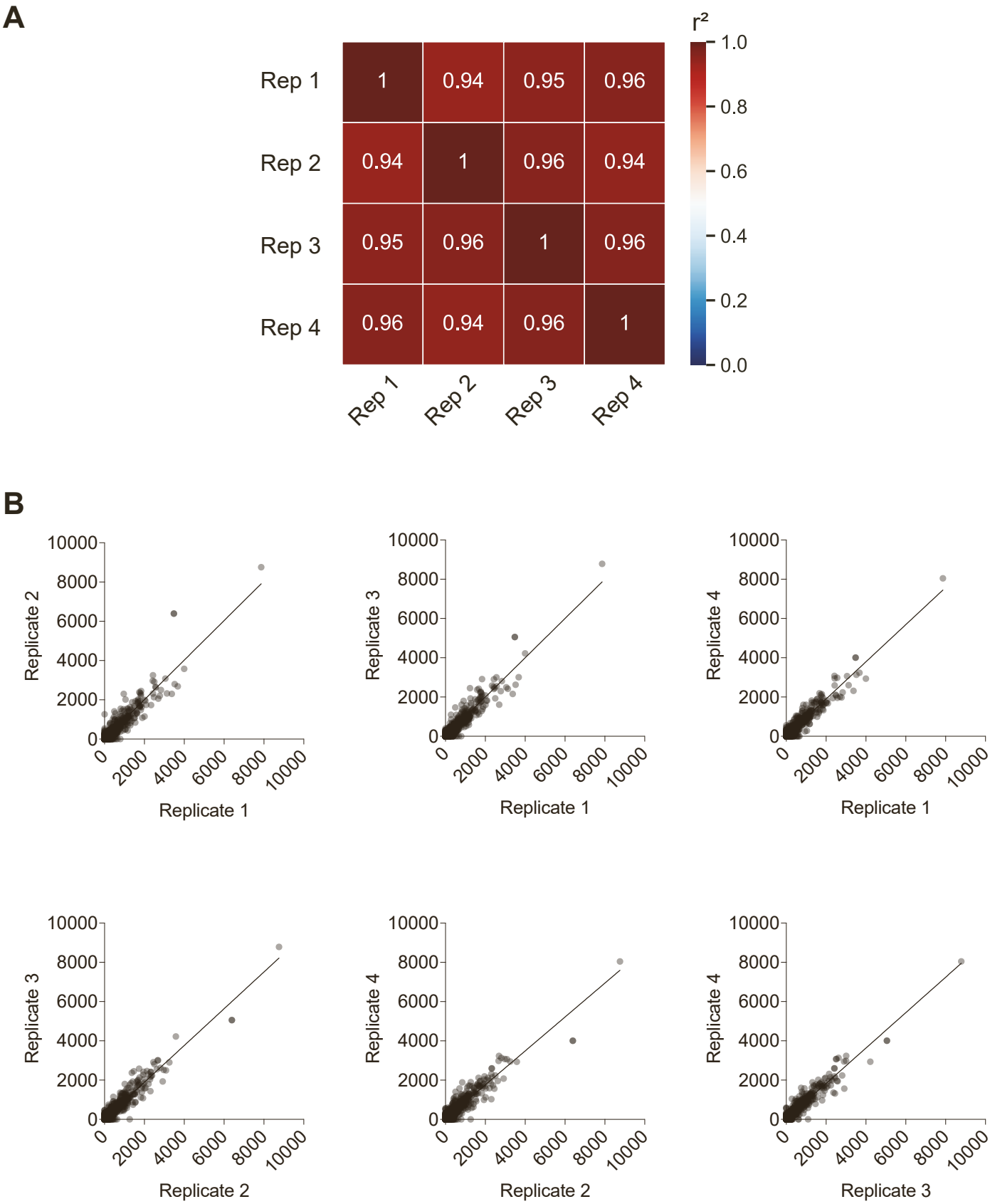

Adhikary et al. Figure S12

Figure S12, Related to Figure 7. Replicates of AP-MS.

(A) Summary table of Pearson correlations for biological replicates of the AP-MS analyses of anti-MCL-1 immunoprecipitates from lysates of wild-type MEFs.

(B) Pairwise scatter plots of normalized spectral abundance factors (NSAFs) for the identified proteins among biological replicates. For all plots, statistical significance of the correlation is $p<0.0001$.

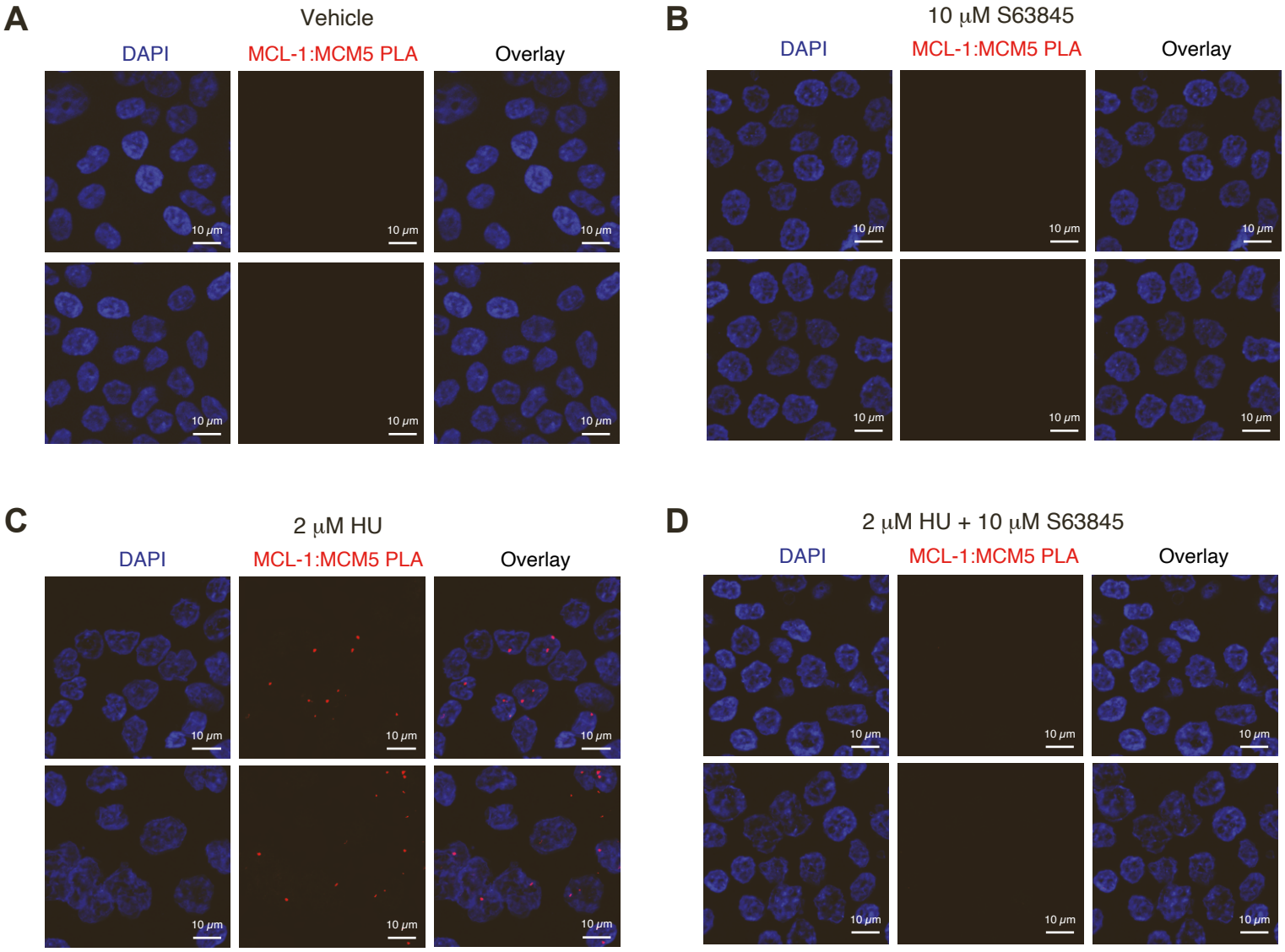

Adhikary et al. Figure S13

Figure S13, Related to Figure 7. Induction of the MCL-1/MCM5 Interaction upon Replicative Stress as Detected by Proximity Ligation Assay.

(A-D) Representative images of MCL-1:MCM5 PLA foci (red) in *Bax*$^{-/-}$*Bak*$^{-/-}$ HCT116 cells subjected to vehicle (0.1% DMSO) (A), 10 μM S63845 (B), 2 μM hydroxyurea (C), or co-treatment with 10 μM S63845 and 2 μM hydroxyurea (D). Nuclei were stained with DAPI (blue).